

DOI: 10.1002/app.50046

ARTICLE

Applied Polymer WILEY

Effect of bone ash fillers on mechanical and thermal properties of biobased epoxy nanocomposites

Md-Jamal Uddin | Deepa Kodali | Vijaya K. Rangari 🗅

Department of Materials Science and Engineering, Tuskegee University, Tuskegee, Alabama, USA

Correspondence

Vijaya K. Rangari, Department of Materials Science and Engineering, Tuskegee University, Tuskegee, AL 36088, USA.

Email: vrangari@tuskegee.edu

Abstract

In this study, the fabrication and characterization of bone ash filled biobased epoxy resin (Super SAP 100/1000, contains 37% biobased carbon content) nanocomposites are presented. Biosource bone ash was modified by size reduction and surface modification processes using a combination of ball milling and sonochemical techniques and characterized using X-ray diffraction, scanning electron microscopy, and transmission electron microscopy. The modified bone ash particles were incorporated into biobased epoxy with noncontact mixing process. The as-fabricated nanocomposites were characterized using various thermal and mechanical analyses. The nanocomposites showed significant improvement in flexural strength (41.25%) and modulus (34.56%) for 2 wt % filler loading. Dynamic mechanical analysis (DMA) results showed improvement in both storage modulus and loss modulus. Additionally, DMA results showed a slight reduction in glass transition temperature which also complies with differential scanning calorimetry results. Thermomechanical analysis results showed a reduction in the coefficient of thermal expansion. Thermogravimetric analysis results showed improved thermal stability at both onset of degradation and the major degradation. These enhanced thermal and mechanical performances of the epoxy nanocomposites allows them to be suitable for lightweight aerospace, automotive, and biomedical applications.

KEYWORDS

biomaterials, biopolymers and renewable polymers, mechanical properties, thermal properties, thermosets

1 INTRODUCTION

Municipal solid waste (MSW) is one of the worst byproducts of urbanization and this urbanization is increasing throughout the world. As the amount of MSW is increasing every day, a substantial portion of plastic waste, is also increasing.^{1,2} Plastic waste is very harmful for human beings, birds and animals, especially the ocean animals.³ The waste plastics impact the global and local sanitation issues and are also responsible for spreading air and water borne diseases.4 Additionally, a large proportion of the plastic waste results in landfill due to lack of recyclability. Even in a properly managed landfill, leachate and landfill, gas emission is must. The discarded plastic pollutes the air and water, and cause complex and long-term effects on animals and human health.^{5,6} Furthermore, greenhouse gases were also produced from the plastic waste, which affect the global climate and thus the environment.

One of the prominent solutions to plastic waste problem is the use of biodegradable polymers. Biodegradable polymers breakdown after their intended purpose or lifetime and result in natural byproducts, such as gases, water, biomass, and inorganic salts.^{7,8} Thus, they are much safer to use in terms of waste point of view. However, biodegradable polymers tend to be weak and most of them are very fragile. Even with the controlled fabrication method, they suffer from specific requirements of mechanical properties for most standard structural applications. Thus, the market of biodegradable polymers is still limited.9 The development of biodegradable materials with comparable properties for standard structural applications can lead to their increased usage. The addition of small amount of fillers, such as clay or nanoparticle fillers, can show significant improvement in mechanical, thermal and barrier properties, flammability resistance and electrical/electronic properties of the final polymer nanocomposite. 10-12 The reason behind this phenomenon is the increased surface area of interaction between the polymer matrix and nano filler. This research is aimed at improving the mechanical and thermal properties of a biodegradable polymer using fillers from natural and renewable sources.

Epoxy resins provide certain benefits over other resin systems. They have an absence of volatiles during curing, good control over the degree of cross-linking, and low shrinkage on curing. Epoxy resins also have excellent chemical, electrical, and heat resistance; high strength, hardness, and impact resistance, and high adhesive strength. Improvements in mechanical and thermal properties have been reported with epoxy nanocomposites reinforced with various fillers and different modifications. 16–28

Biodegradable polymers, on the other hand, lack mechanical strength, as stated earlier. Since epoxies have very high mechanical strength, and biodegradable polymers have less, a biodegradable epoxy resin may have sufficient strength required for typical structural applications. Compositing the biodegradable epoxy polymer with fillers can lead to much improved strength and other properties. Masoodi et al.²⁹ reported better mechanical properties at lower percentages of cellulose nanofiber in cellulose nanofiber filled biobased epoxy nanocomposites. Hoto et al.³⁰ studied the flexural behavior and water absorption of sandwich composites from natural fibers and cork core. They concluded that the green composite-based sandwich could be one of the useful alternatives to the traditional ones.

Synthetic fillers, such as glass fiber and carbon fiber impose severe health hazard during both the production and processing of the fibers. The chemicals that are involved in the production of synthetic fillers needed to be discarded and disposed properly. Use of synthetic fillers thus impacts the environment and health. On the other hand, natural fibers, especially those from renewable sources, are much safer for health and the environment. Also, a lot of them are biodegradable in nature.³¹

Animal bones, such as chicken bones and others, are one of the most common everyday wastes. The primary constituents of bones are calcium phosphates and their derivatives, all of which are very hard in terms of mechanical properties. When they are incorporated into a polymer matrix, they strengthen the structure by filler effect. When these nanoparticles are added to the polymer matrix, the surface to volume ratio of the composite becomes very high, typically in the order of one magnitude higher than the traditional composites. This increased surface interaction leads to higher entanglement crosslinking of the polymer chain when they are subjected to stress. The resulting strength is thus found to be higher than that of the polymer itself. Jaggi et al.³² studied the structural and mechanical response of high density polyethylene filled with hydroxyapatite (Hap), a calcium phosphate mineral found in bones. They found that the tensile and flexural properties increased and impact strength decreased linearly with Hap content; the yield stress remained unaffected. Other researchers working with Hap found similar results.33-35 Hong et al.36 studied the composites of poly (lactide-co-glycolide) (PLGA) and the surface-modified Hap nanoparticles. The composites showed better tensile strength and improved elongation at break in the filler percentage range of 2%-15%. Especially at 15 wt% of filler loading, the PLGA/ HAP composite showed about 20% higher tensile strength than the neat PLGA materials. Asuke et al.³⁷ studied the effect of bone particle on the properties of polypropylene/bone ash composites. They reported increase in hardness values, compressive, tensile, and flexural strength. Other researchers working with thermoplastic polymer composites have found similar results.³⁸⁻⁴⁴ They found that the composites show better properties at 5-15 wt% of filler particle addition. For optimum properties, they suggested that the filler percentage should not exceed 15%.

Animal bone-based particles and bone ashes are hard and brittle in nature. When they are incorporated into a polymer matrix, they strengthen the structure by filler effect. Owing to the nature of high surface to volume ratio of nanoparticles, they tend to form agglomerations. Hence, nanofiller dispersion and interfacial interaction between polymer and nanofiller persists as major challenges in synthesizing the epoxy nanocomposites.

Especially, the inhomogenous dispersion of the nanofillers may reduce the strength of the epoxy nanocomposites. 46–48 In order to overcome these challenges, various mixing methods, such as high speed mechanical stirring, magnetic stirring, shear mixing, and ultrasonic horn mixing (ultrasonication), are employed and these methods proved to be effective in obtaining homogenous dispersion. 49,50

Although epoxy-based nanocomposites are widely studied systems, the studies on biobased epoxy nanocomposites with sustainable natural fillers are relatively underexplored. Biobased epoxy polymers are as good as other traditional epoxy polymers. With the addition of natural fillers, their properties can be further enhanced as compared to that of conventional nanocomposites. Thus, this work focuses on the development of biobased epoxy nanocomposites with comparable mechanical and thermal properties as of traditional ones.

In this work, we present the preparation and characterization of sustainable waste bone ash nanoparticles-reinforced biobased epoxy (Super SAP 100/1000, contains 37% biobased carbon content) nanocomposite. The bone ash particles are subjected to ballmilling followed by ultrasonication to reduce the particle sizes. These nanoparticles are then dispersed in biobased epoxy resin using ultrasonication and noncontact mixing to produce uniform dispersions and cured at room temperatures. The thermal and mechanical properties indicate that these nanocomposites can be used in aerospace, automotive, and coating applications.

2 | MATERIALS AND METHODS

2.1 | Materials

For the development of the polymer nanocomposites, a biodegradable epoxy resin with 37% biobased carbon content was used. The resin used was Super Sap® 100/1000 epoxy; a two-part epoxy resin system purchased from Entropy Resins Inc. Part A was Super Sap® 100 Epoxy, a modified, liquid epoxy resin; part B was Super Sap® 1000 Hardener. As opposed to traditional epoxies that are primarily composed of petroleum-based materials, Super Sap® formulations contain bio-renewable materials sourced as coproducts or from waste streams of other industrial processes, such as wood pulp and bio-fuels production. These natural components have excellent elongation and exceptionally high mechanical properties. The filler, bone ash, was purchased from Laguna Clay Company, Florida. The purchased bone ash was obtained from calcination of animal bones. Decahydronaphthalene (Decalin) was used for functionalizing nanoparticles with ultrasonication. Decalin was obtained from Sigma-Aldrich Inc.

2.2 | Modification of the nanoparticles

Ball milling is a top-down method that utilizes mechanical attrition to synthesize nanoscale materials. In this

TABLE 1 Different labels of nanoparticles and nanocomposites

Nanoparticle	Description	Relevant nanocomposite
BARW	As collected, raw bone ash	SS/BARW
BAM10	Bone ash ball milled for 10 hours	SS/BAM10
BAMS	Ball milled and sonicated bone ash	SS/BAMS
(No filler)	No filler condition	SS/neat

Abbreviations: BARW, bone ash; SS, Super Sap.

work, a vibratory ball mill, 8000D mixer/mill from SPEX SamplePrep, with Zirconia vials and balls was used to produce nanoparticles. The as collected bone ash (labeled BARW) was ball milled in dry condition. Two separate zirconia ceramic vials of 45 ml (6.35 cm diameter, 6.8 cm long), each with two zirconia balls (12.7 mm diameter) were loaded with precursors of weight 5 gm. Then the ball mill was allowed to run for 10 h. After carefully separating the fine powder, they were dried, stored, and labeled as BAM10.

Ultrasonic irradiation is a well-known technique for nanoparticle synthesis as well as for chemical reactions. The most important aspect of ultrasound irradiation is cavitation—the formation, growth, and implosive collapse of bubbles in a liquid. When such a cavity forms and collapse, it produces an immense localized energy that drives the chemical reaction to happen or breaks the agglomerated particles into smaller particles. In this work, a Sonics vibra cell ultrasound, modeled as WCX 750 with an ultrasonic liquid processor of 750 W output with 20 kHz, 100 W/cm² converter and a flat titanium horn of 19 mm in diameter was used. The ball milled bone ash powder, BAM10, is dispersed in decalin (1 gm in 50 ml), and the solution was ultrasonicated for 3 h using 50% amplitude. After sonication, the solution was washed with ethanol and centrifuged at 5000 rpm. After the removal of the solvent, the precipitate was vacuum dried for 24 h to obtain the final nanoparticle (labeled BAMS). The nanoparticles that were obtained during the process were labeled along with their corresponding nanocomposites in Table 1.

2.3 | Development of the nanocomposites

Nanoparticles were first introduced into the polymer, part A of the epoxy composite. To prevent

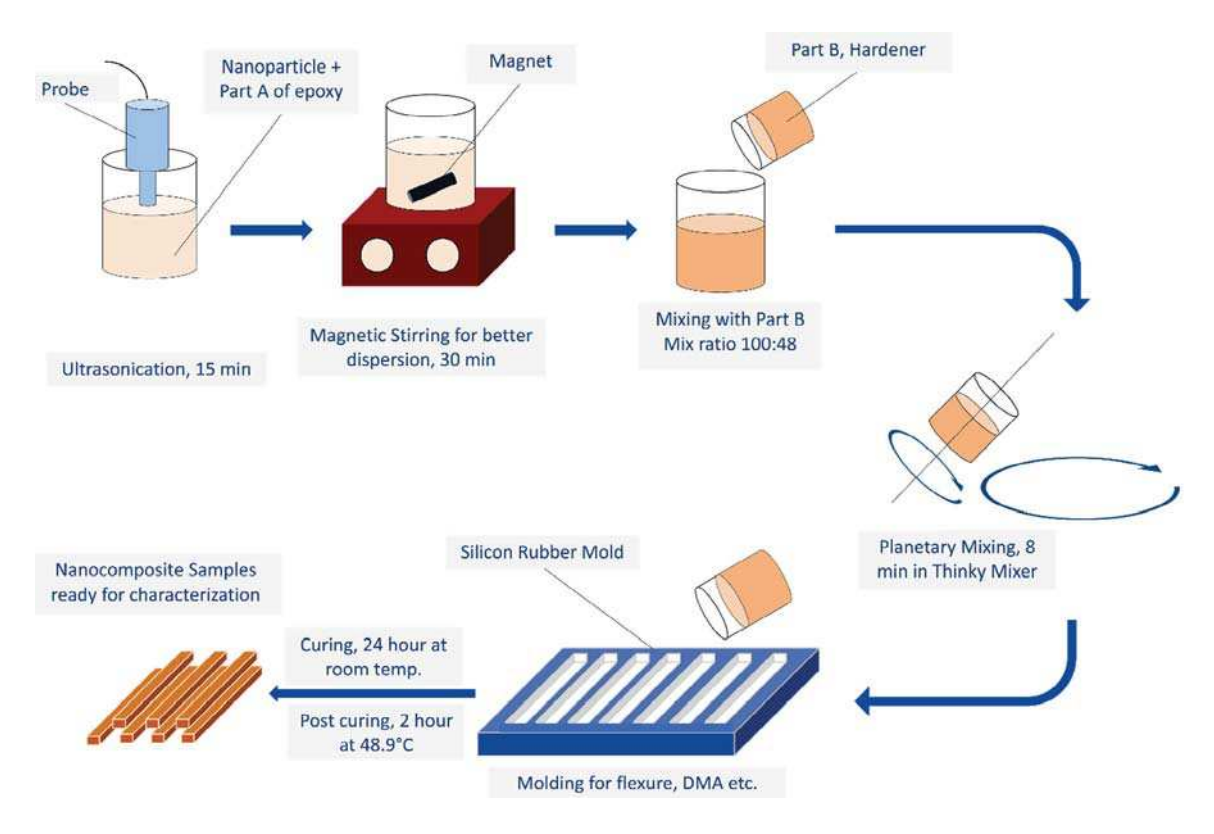


FIGURE 1 Nanocomposites development process [Color figure can be viewed at wileyonlinelibrary.com]

agglomeration of the particles, the mixture was ultrasonicated for 15 min using a 2:1 on-off cycle with 50% amplitude. For effective dispersion, they were stirred in a magnetic stirrer for 30–45 min. Finally, the part B of the epoxy, the hardener was added in a ratio of 100:48 for part-A: part-B. The mixture was then mixed (2000 rpm, 5 min) and degassed (2200 rpm, 3 min) in a planetary noncontact mixer (Thinky mixer, ARE-250).

The mixer was then carefully poured in the silicon rubber molds for flexure and dynamic mechanical analysis (DMA) (size compliant with ASTM standard) test and was left to cure at room temperature for 24 h. Post curing was done for 2 h at 48.9°C in the oven. After air cool to room temperature for 3 h, the specimens were finished to meet specific dimensions for characterization and stored. Figure 1 shows the nanocomposite development process.

The synthesized nanoparticles and nanocomposites were characterized using X-ray diffraction (XRD), flexure, thermogravimetric analysis (TGA), differential scanning calorimetry (DSC), thermomechanical analysis (TMA), DMA scanning electron microscopy (SEM) and transmission electron microscopy (TEM). For XRD, a Rigaku-DMAX-2000 X-ray diffractometer was used at 40 KV and 30 mA, 5°C/min sampling rate, and 0.020 sampling width from 3° to 80° 2θ angles. For flexure, a

Zwick/Roell Z2.5 materials testing system with 2.5 kN load cell was used.

For specimen size, strain rate, and other experimental parameters, ASTM D790 standard was followed.⁵¹

For TGA, a thermogravimetric analyzer, Q-500 from TA Instruments, was used. The composites were heated up to 650°C at a rate of 5°C/min in nitrogen environment. For DSC, we used a differential scanning calorimeter, Mettler Toledo, with a heating rate of 5°C/min up to 200°C in nitrogen environment. For DMA, a dynamic mechanical analyzer, Q-800 from TA Instruments was used with a heating rate of 5°C/min up to 140°C in nitrogen environment. The vibration frequency was 1 GHz in nitrogen flow of 50 ml/min. The mode of loading was double cantilever. For TMA, a thermomechanical analyzer, Q-400 from TA Instruments was used with a heating rate of 5°C/min up to 150°C in nitrogen environment. This test was done according to ASTM standard. ⁵²

For SEM, a JEOL JSM-7200F field emission scanning electron microscope (FESEM, JEOL USA, Peabody, MA) was used. The samples were sputter coated with gold/palladium (Au/Pd) for 3 mins at 10 mA using Hummer sputter coater prior characterization. For TEM, a JOEL 2010 TEM was used. Nanoparticles were first dispersed in ethanol and then dispensed on Cu grid and air dried. This copper grid was further used for TEM analysis at an operating voltage of 200 kV.

3 | RESULTS AND DISCUSSION

3.1 | Characterization of the nanoparticles

Calcium phosphate and calcium carbonate are the main constituents of the mineral part of the bone. The calcination of bone results in calcium phosphate and its mineral forms in bone ash. Figure 2(a) shows the XRD pattern of BARW. The pattern matches with Monetite-CaHPO₄ (JCPDS-Pdf #70–0360) and Brushite-CaHPO₄(H₂O)₂ (JCPDS-Pdf #72-0713), and confirms that the as collected bone ash is comprised of brushite and monetite-two calcium phosphate minerals. X-ray pattern clearly shows that BARW contains brushite and monetite only, and there is no other phase of calcium phosphate or impurities present. Brushite is a calcium phosphate mineral and monetite is the anhydrous variation of brushite. When stored at room temperature for more than 3 days, brushite starts to react and converts into monetite.⁵³ The literature suggests that the low-density chicken bone ash contains mostly brushite.⁵⁴ When stored, this brushite can convert to monetite and thus can be found as a combination of both of them, as is found in our work.

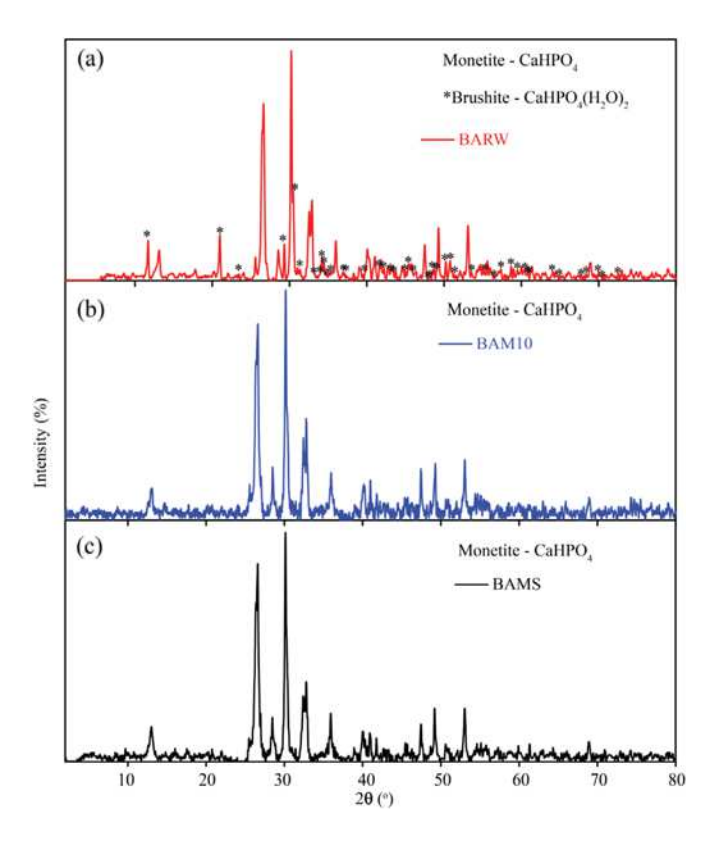


FIGURE 2 X-ray diffraction patterns of (a) bone ash (BARW) (b) BAM10 and (c) BAMS [Color figure can be viewed at wileyonlinelibrary.com]

Ball milling technique is a powerful and effective method to reduce the particle size. The enormous energy exerted by the collision of ball-to-ball and ball-to-wall break down the particles into smaller sizes. Ball milling was carried out in order to reduce the particle size of bone ash. Figure 2(b) shows the XRD pattern of bone ash ball milled for 10 h (BAM10). As found in the X-ray analysis, monetite is the only phase present in compound BAM10. This is because the energy exerted during ball milling may have triggered the conversion reaction of brushite into monetite. Figure 2(b) also shows that there are no other impurities present. This is supported by the fact that bone ash milled in dry condition in ceramic vials and balls, and thus, there were no impurities from the ball-ball in mill process.

Ball milled particles are generally irregular in size and shape, and the size distribution is also varied. The overall yield of smaller sized particles is lower in ball milling than other techniques. When particles are ball milled for a prolonged period, it may also result in the agglomeration of the particles due to the enormous surface energy at particle surfaces. Ultrasonication, on the other hand, can reduce the particle size further. This process is more localized than milling. In our work, a combination of ball milling and ultrasonication was used to synthesize the bone ash nanoparticles (BAMS). Ultrasound irradiation was followed by ball milling.

Figure 2(c) shows the XRD pattern of the synthesized bone ash particles by ultrasonication followed by ball milling (BAMS). As shown in this pattern, only monetite is present, which indicates that there is no other phase or impurities. This also shows that sonication did not cause any amorphization or the chemical structural changes.

Debye-Scherrer formula is a widely accepted method to determine crystallite sizes for crystalline material. Although the error percentage is relatively high, this method can be used as a qualitative measurement very accurately. This method uses the full-width-half-maxima (FWHM) to calculate the crystallite size as shown in the equation below.

$$\tau = \frac{K\lambda}{\beta \cos \theta}$$

where τ is the mean size of the ordered crystallites; K is a dimensionless shape factor, typically 0.9; λ is the X-ray wavelength; β is the line broadening at half the maximum intensity (FWHM), in radians; θ is the Bragg angle.

Analyzing the pattern of BARW in Figure 2(a), 100% XRD peak for (-120) plane, the estimated crystallite sizes using Debye Scherrer formula were found to be 32.2 nm. Figure 2(b) shows that ball milling has caused the peak widening in the X-ray pattern. This indicates that the

particle size reduction has occurred. Calculating the FWHM for the 100% X-ray peak at (-120) plane gives that the particle size after ball milling is 28.4 nm. Sonication has also caused the peak widening in the X-ray patterns, which indicates further particle size reduction. Using the Debye–Scherrer formula and FWHM method, the estimated crystallite sizes of BAMS (Figure 2(c)) were found to be 27.6 nm.

To determine the particle size, shape, and distribution, and to examine the crystallinity, SEM and TEM analysis were used. Figure 3(a) shows the SEM image of the as received bone ash. Based on the micrograph presented, the particles are relatively large in size and their shapes are much irregular. Furthermore, the particles are highly agglomerated. Figure 3(b),(c) shows the SEM images of synthesized bone ash particles (BAMS) and its expanded view, respectively. The micrographs confirm that the size reduction of bone ash via ball milling and ultrasonication was successful and as such the particles are much smaller in size and highly porous. Additionally, the particle agglomeration is reduced. Essentially, particle size distribution is observed to be much more even.

The TEM micrograph of the as received bone ash was shown in Figure 3(d). The micrograph reveals the lattice planes of bone ash particles, which suggests that bone ash is highly crystalline and these results are consistent with XRD patterns. The micrographs of synthesized bone ash particles and its magnified view are shown in Figure 3(e),(f), respectively. The micrographs suggest that the particles retain their crystallinity after ball milling and sonication. The particle size is reduced to \sim 25 nm, and these particles are regular in shape.

3.2 | Characterization of the nanocomposites

3.2.1 | Mechanical properties of the nanocomposites

Flexural properties like strength and modulus of all nanocomposite systems were evaluated in this study. Flexural characterization was carried out using a three-point bending test according to the ASTM standard D790. Figure 4(a) shows the stress-strain curve of neat Super

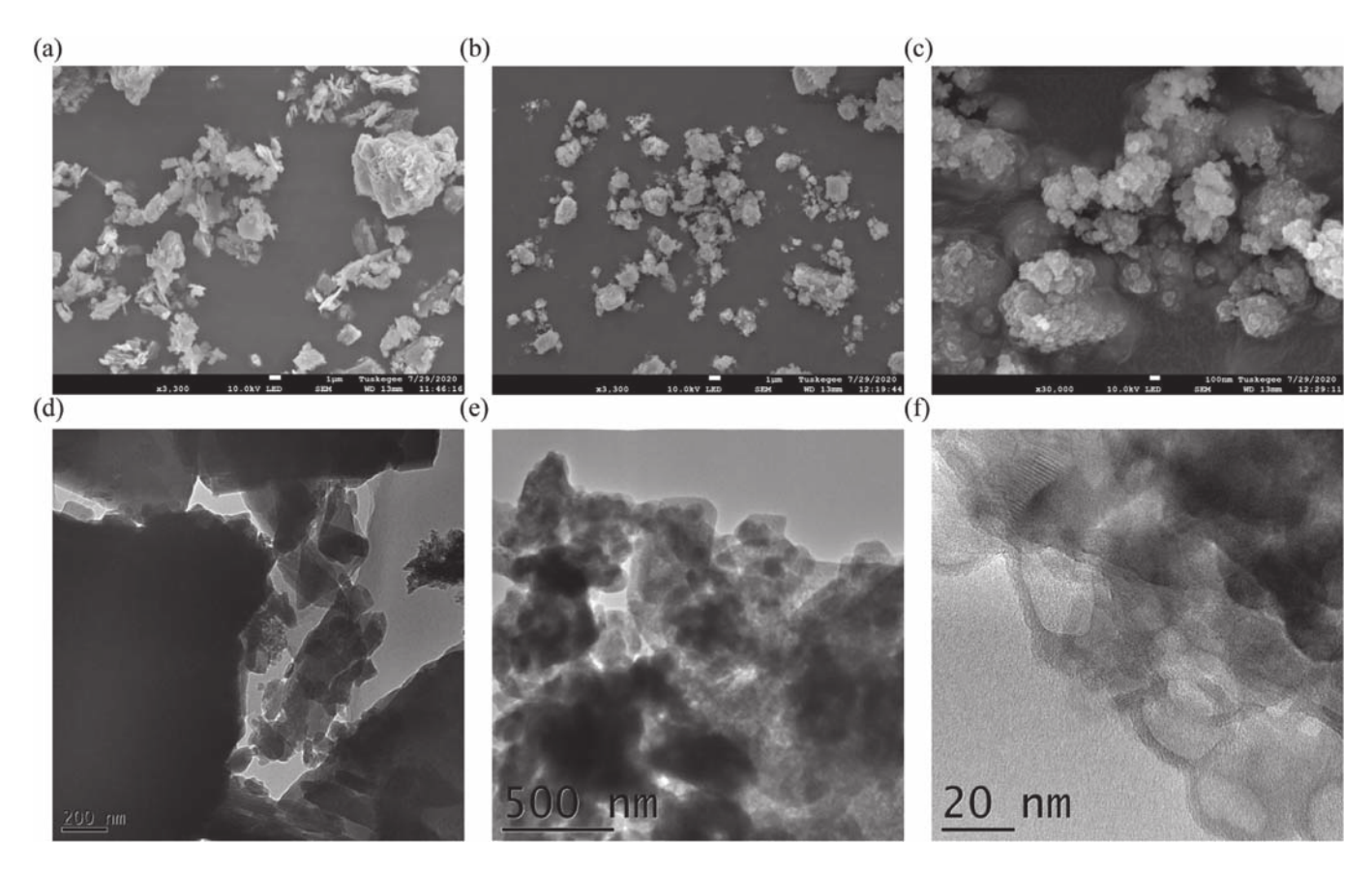


FIGURE 3 Scanning electron microscopy (SEM) and transmission electron microscopy (TEM) micrographs of bone ash nanoparticles (a), (d) as it is condition, BARW (b), (e) final synthesized condition, bone ash (BAMS), and (c), (f) BAMS in higher resolution, respectively [Color figure can be viewed at wileyonlinelibrary.com]

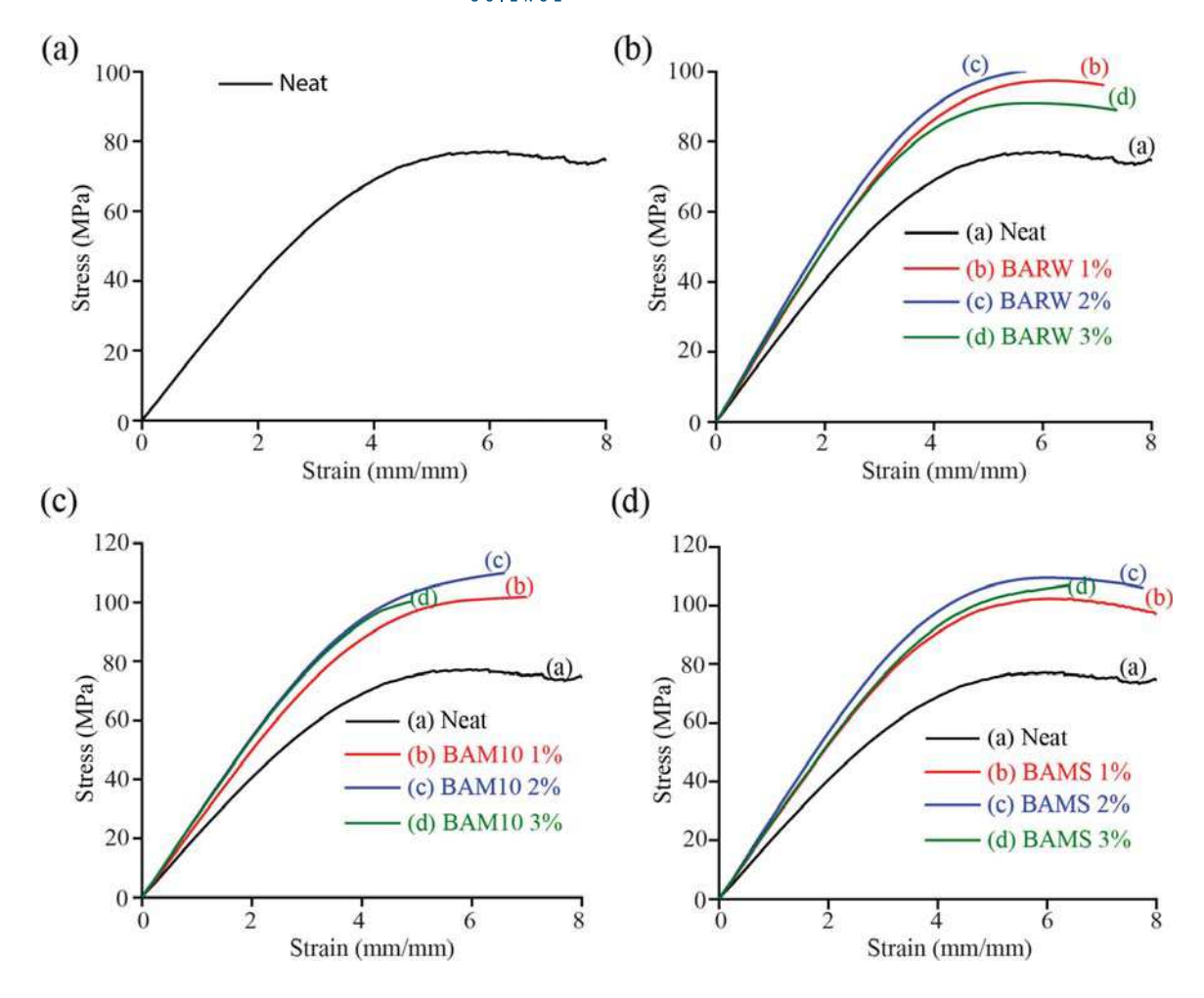


FIGURE 4 Flexure behavior of the nanocomposites (a) Super Sap (SS)/neat, (b) SS/BARW, (c) SS/BAM10 and (d) SS/BAMS [Color figure can be viewed at wileyonlinelibrary.com]

TABLE 2 Flexural properties of SS/neat

	SS/neat, as developed	Manufacturer specification
Elongation (%)	6.05	7
Flexural modulus (GPa)	1.95	2.3
Flexural strength (MPa)	77.48	77

Abbreviation: SS, Super Sap.

Sap 100/1000 epoxy resin system (SS/neat). The findings from the stress–strain curve of the neat epoxy system has been summarized and compared with manufacturer's specification in Table 2. Flexural data of SS-neat showed that the neat epoxy did not fail within 5% of the strain. This indicates that the epoxy is considerably ductile in nature, and it requires special considerations for flexural characterization. As suggested by the ASTM standard D790B, we used an increased strain rate to run flexural test of these nanocomposites. The actual strain rate used is 20 mm/mm/sec which is 10 times more than the rate

used for D790A. Also, we considered the strain at maximum flexural strength to compare ductility of the nanocomposite systems as suggested in ASTM standard D790.

Table 2 shows that our experimental findings for flexural properties are very close to the manufacturer's specification. This ensures that our processing route and characterization techniques comply with the industry standard. Thus, the skill level used in this work and the quality of this work also comply with industry standard.

Figure 4(b) shows the flexural behavior of the Super Sap 100/1000 nanocomposite systems with as received bone ash as a filler (SS/BARW) in 1%, 2%, and 3% loading. As seen from the curve, flexural strength, modulus, and toughness are improved for every nanocomposite compared to the neat epoxy system subjected to the same processing and testing environment. However, maximum improvement in flexural strength and modulus were found for 2% bone ash filler loading in the nanocomposite.

TABLE 3 Flexural properties of nanocomposites

	Filler amount wt%	Strain at maximum stress %	Maximum stress MPa	Flexure modulus GPa	Percentage increase in strength, %	Percentage increase in modulus, %
SS/neat	0	6.05	77.48	1.95	0.00	0.00
SS/BARW	1	6.18	97.42	2.23	25.73	14.49
SS/BARW	2	5.93	100.43	2.47	29.62	26.67
SS/BARW	3	5.55	91.01	2.36	17.47	20.92
SS/BAM10	1	6.03	100.76	2.32	30.05	18.97
SS/BAM10	2	5.41	104.95	2.60	35.46	33.22
SS/BAM10	3	4.61	99.28	2.52	28.13	28.97
SS/BAMS	1	6.13	102.58	2.50	32.39	28.33
SS/BAMS	2	6.00	109.44	2.62	41.25	34.56
SS/BAMS	3	5.71	104.67	2.52	35.09	29.23

Abbreviations: BARW, bone ash; SS, Super Sap.

After ball milling of bone ash, the particles were used as filler to develop nanocomposites in Super Sap 100/1000 epoxy (SS/BAM10). Figure 4(c) shows the flexural behavior of SS/BAM10 nanocomposite systems with filler loading of 1%, 2%, and 3% of ball milled bone ash (BAM10). The flexural strength, modulus, and toughness are improved for the nanocomposites compared to the neat epoxy system. Maximum improvement in flexural strength and modulus are found for 2% BAM10 filler loading in the nanocomposite. Bone ash was also ultrasonicated after dry ball milling of 10 h. The final synthesized bone ash particles (BAMS) were also infused into Super Sap 100/1000 epoxy polymer as a filler to develop nanocomposites. The resulting nanocomposites (SS/BAMS) are characterized for flexural properties which are shown in Figure 4(d). It shows that the flexural strength, modulus, and toughness are improved for the nanocomposites compared to the neat epoxy system. Again, the maximum improvement in flexural strength and modulus are found for 2% of filler loading in the nanocomposite.

Table 3 summarizes the flexural properties of bone ash filled nanocomposite systems. It is found that the flexural strength and modulus has increased for all three different variations of bone ash particles as compared to the neat system. The ball milled and sonicated bone ash filled nanocomposites (SS/BAMS) exhibits superior strength and modulus followed by the ball milled bone ash filled nanocomposites (SS/BAM10) and the as received bone ash filled nanocomposites (SS/BARW) sequentially. This is attributed to the corresponding decrease in the particle sizes in the three bone ash based nanoparticles, which in turn has increased the surface area of the nanoparticles.⁵⁵ Hence, there is increased interaction in filler–polymer interface, which further improved the resistance to mechanical loading.

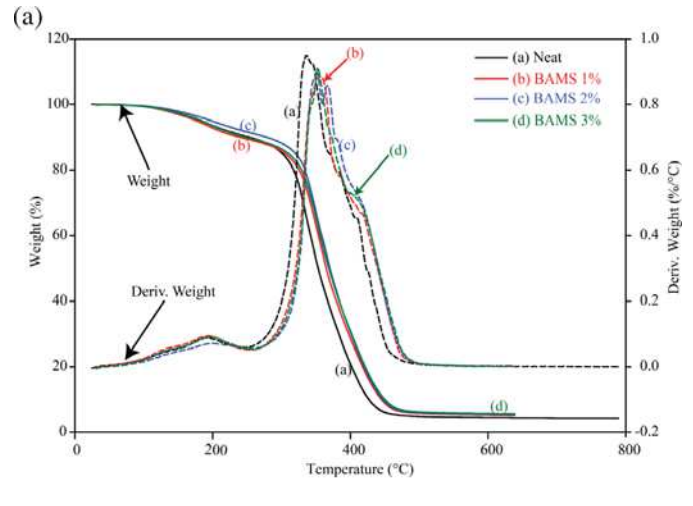
The flexural strength is improved up to 41.25%, and flexural modulus is improved up to 34.56% for 2% BAMS filler loading in the SS/BAMS system as shown in Table 3. Although the flexural strength and modulus is increased, strain at maximum stress does not show any significant change. This has resulted in an overall increase in toughness of the final nanocomposite, SS/BAMS at 2% filler loading.

The results clearly show that, the flexural strength and modulus have improved as compared to the neat epoxy system subjected to the same processing and testing environment. However, for most of the nanocomposites, the strain at maximum stress remains almost the same. This behavior suggests that the ductile behavior of Super Sap 100/1000 epoxy polymer is not influenced much with the addition of nanoparticles as filler. This is particularly interesting, because it suggests that the structural interaction between fillers and the matrix has only influenced to improve the flexural strength and modulus of the nanocomposites whereas the strain to maximum strength is not changed. For inorganic particles, such as for the nanoparticles from bone ash, it can be explained in a fairly simple way. The interaction between the particles and matrix was only the physical effect of filler addition; there was no crosslinking or chemical bonding between them. Similar findings have been reported by other researchers with bone ash based nanoparticles. 32,37,47

3.3 | Thermal properties of the nanocomposites

3.3.1 | Thermogravimetric analysis

The effect of the various natural fillers on the thermal stability of the nanocomposites has been studied by TGA. The



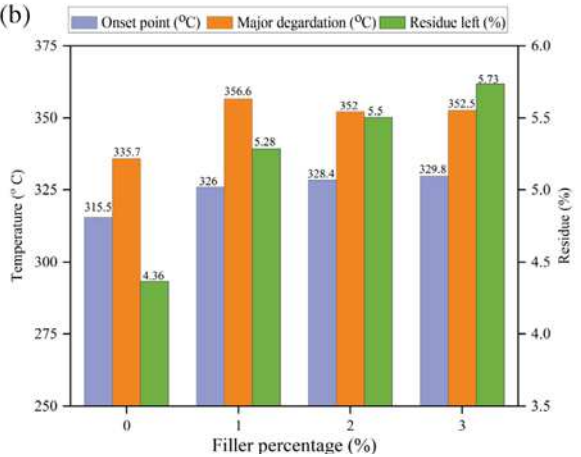


FIGURE 5 Summary of thermogravimetric analysis: (a) thermogravimetric analysis (TGA) thermographs of the nanocomposites and (b) summary of the results of the analysis [Color figure can be viewed at wileyonlinelibrary.com]

onset temperature to the major degradation, the major degradation temperature and amount of residue have been measured to evaluate the effect of the fillers. Figure 5(a) shows the TGA weight loss and derivative weight loss curves of BAMS-filled nanocomposites, SS/BAMS, with varying amount of fillers (1%, 2%, and 3%). As seen from the curves, both the onset temperature and the major degradation temperature of SS/BAMS were improved as compared to SS/neat as shown in Figure 5(b). Thus, the thermal stability of the nanocomposite was improved. Also, as the filler content increases, the temperatures also increase.

Figure 5(b) summarizes the important TGA results of SS/BAMS nanocomposites with 1%, 2%, and 3% of filler loading. It shows the onset temperature to major degradation and the major degradation temperature for each nanocomposite has increased with increasing filler percentages. These shows that the nanocomposites loaded with bone ash are thermally more stable than the neat system, SS/neat. The figure also shows that the amount

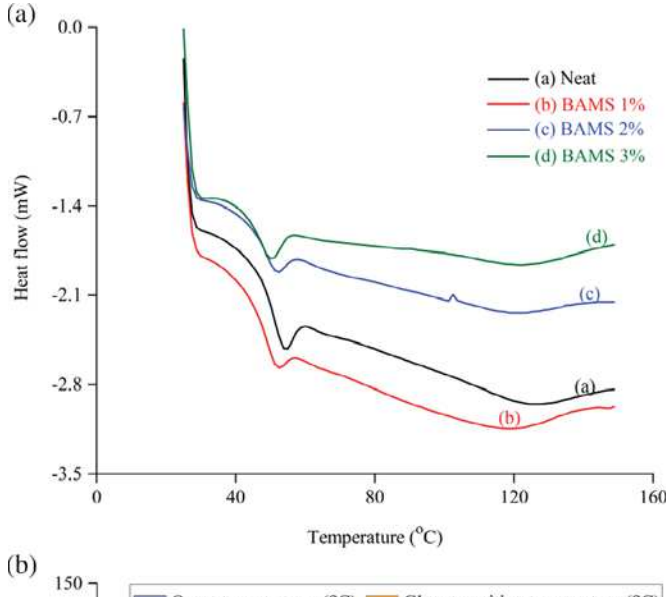
of residue left has increased as compared to the neat epoxy system. This indicates that the fire retardant ability of the composite has increased. The onset temperature has improved ranging from 10 to 15°C, and the major degradation has improved from 8 to 25°C. This is primarily attributed to the higher thermal stability of the bone ash ceramic nanoparticles in the nanocomposites. The bone ash nanoparticles that are not in direct contact with the polymer, shield the heat energy from rapid transfer to the polymer and thus block thermal degradation. 48,56

3.3.2 | Differential scanning calorimetry

Figure 6(a) shows the DSC heating curves of SS/BAMS with 1%, 2%, and 3% loading of the filler synthesized from bone ash. The DSC results are summarized in Table 5. As seen from the curves, both the onset temperature and the glass transition temperature of SS/BAMS were not much improved as compared to SS/neat. Thus, the overall cure dynamics of Super Sap 100/1000 is not changed for nanoparticles filled composites.

Figure 6(b) summarizes the DSC data of the SS/BAMS nanocomposites, comparing with the neat system (0% filler), SS/neat. The glass transition temperature of the 2% SS/BAMS is higher compared to the 1% and 3% filler systems and is closer to the SS/neat. As seen from the chart in Figure 6(b), the overall cure behavior of Super Sap 100/1000 epoxy is not changed for any percentages of the filler. To find the reason of this phenomenon, we have to look at the structure and cure behavior of Super Sap 100/1000 epoxy neat polymer.

Super Sap 100/1000 is a biobased epoxy which contains 37% biobased content, the remaining major portion of the polymer is petroleum-based content. For its biobased contents, there is a minor decomposition in TGA behavior of the polymer at around 200°C (Figure 5). The major degradation is, however, from the petroleum-based content. The same biobased content that shows the minor decomposition in Figure 5 probably undergoes a melting or similar phase change at around 50°C, as shown in Figure 6. This causes an endothermic reaction in a temperature range from 50 to 60°C, which is evident in all DSC plots. This biobased content also most possibly acts as a plasticizer. Plasticizers are small molecule chains that inhibit the cross-linking in a thermoset polymer by staying in between the polymer chains and thus increase the plasticity (ductility) of the polymer. The biobased content that acts as a plasticizer is also responsible for the extensive ductility of the Super Sap 100/1000 polymer as evident in flexure test. The presence of this content has prevented any kind of structural integration (such as cross-linking in between the polymer) that was



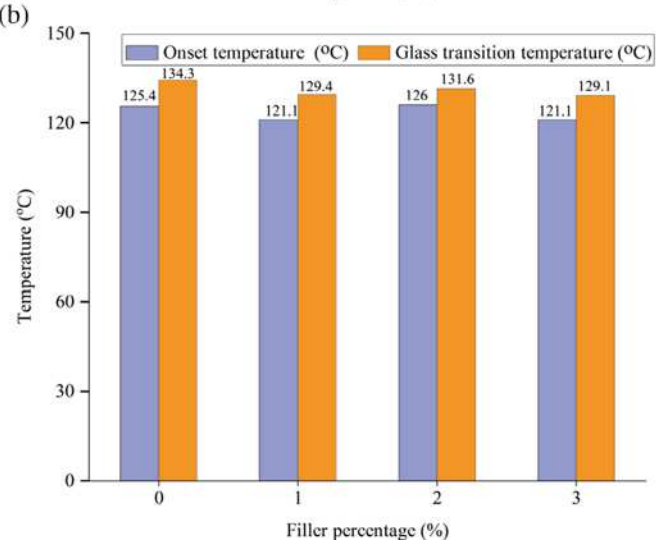


FIGURE 6 Summary of differential scanning calorimetry (DSC) analysis: (a) DSC heating curves of the nanocomposites and (b) onset temperatures and glass transition temperatures for various filler percentages [Color figure can be viewed at wileyonlinelibrary.com]

expected for the presence of fillers in the nanocomposites. Thus the fillers, only might have the mechanical filler effect due to their excessive hardness, thermal stability and particle properties. The improvement of most of the mechanical and thermal properties of the nanocomposites is not due to the enhanced polymer cross linking rather may be due to the better particle dispersion in the polymer matrix.

3.3.3 | Thermomechanical analysis

The effect of natural fillers on the dimensional stability of the nanocomposites were studied by comparing the coefficient of thermal expansion (CTE) in TMA using the expansion mode. Figure 7(a) shows the dimensional change of bone ash filled nanocomposites, SS/BAMS, with temperature for varying (1%, 2%, and 3%) filler percentages. These results are summarized in Figure 7(b). CTE of the composites are determined as a measurement of dimensional stability of the composites from the slope of the curves both before (30–70°C) and after (110–140°C) the glass transition temperature (T_g). As seen from the curves, the CTE of the composites are decreased both before and after the T_g as compared to the neat system, SS/neat. Thus, the overall dimensional stability of SS/BAMS is improved. However, T_g itself is not much changed.

CTE of the nanocomposites before T_g were decreased up to 64% as compared to the neat polymer, regardless of the filler content loading. Thus, the dimensional stability of the nanocomposites has improved. CTE after T_g is also improved for all the nanocomposites, up to 18%. However, the T_g is not changed significantly. As seen from the chart, maximum improvement in terms of dimensional stability is found for 1% loading of BAMS. The decrease in CTE of the nanocomposites can be attributed to the high stiffness of the bone ash nanoparticles. Reinforcing fillers that are hard and stiff in nature are also highly resistant to deformation. When nanocomposites are subjected to the thermomechanical load, this nature of the nanoparticles causes a resistance to strain near the particles, as a result of the particle-matrix interface interaction. 56,57 This results in an overall reduction in the strain of the composite, and thus an increase in the dimensional stability. The absence of any kind of improvement in T_g is attributed to the notion that the Super Sap 100/1000 epoxy polymer contains some biobased content which has been described and discussed earlier.

3.3.4 | Dynamic mechanical analysis

DMA is used to characterize the viscoelastic behavior of the polymer in terms of storage modulus, loss modulus, and damping. Figure 8(a) shows the viscoelastic behavior of bone ash filled nanocomposites, SS/BAMS, with 1%, 2%, and 3% of filler loading. Storage modulus is found to be improved for both 1% and 2% of filler loading. Loss modulus is improved for all percentages of filler loading. Glass transition temperature (T_g) of the nanocomposite, both by tan delta and loss modulus are not improved. However, the change in T_g is not significant.

Figure 8(b) summarizes the storage modulus, loss modulus, and damping behavior of all the nanocomposites. As seen from the Figure 8(b), maximum improvement for the storage modulus was found for 2% filler loading in SS/BAMS which complies with the results for flexural

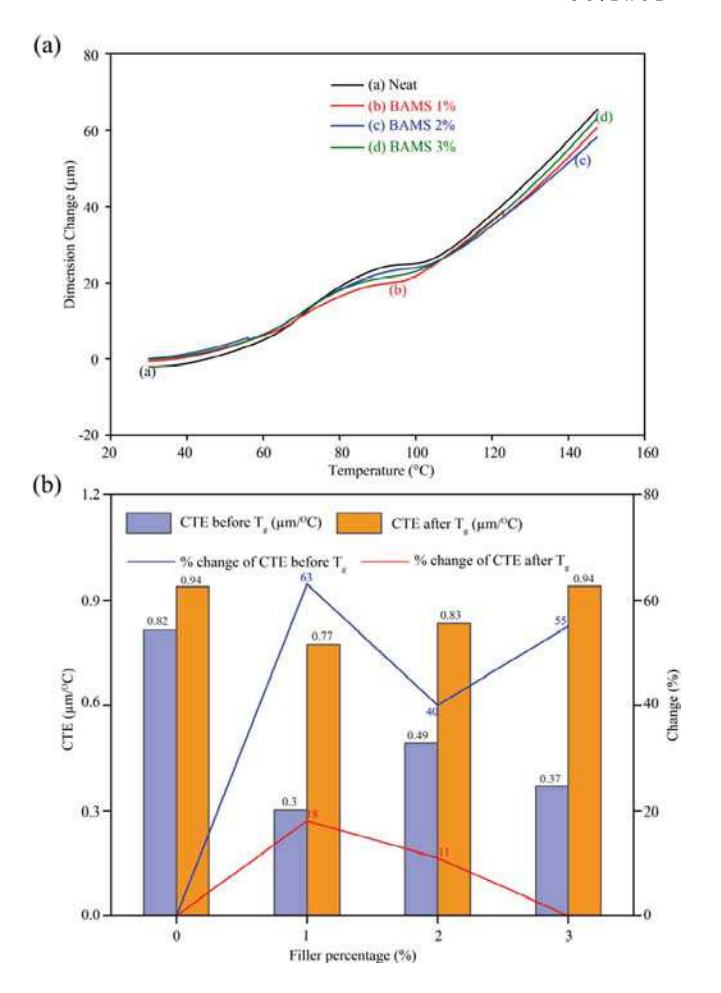


FIGURE 7 Summary of thermomechanical analysis (TMA) analysis: (a) TMA curves of the nanocomposites and (b) summary of the results for various filler percentages [Color figure can be viewed at wileyonlinelibrary.com]

strength. Improvement in the loss modulus was found to be same for all percentage of filler. T_g of the nanocomposite, both by tan delta and loss modulus are not much changed. The improvement in storage modulus is attributed to the mechanical stiffness, hardness, and high thermal stability of the reinforcing fillers. In DMA, as the temperature is increased, the abovementioned filler properties cause the heat energy to be localized within and around the particles. Thus, the matrix which is in contact with the particles or around the particles is shielded from heat transfer between themselves and the particles. Improvement in the storage modulus can also be attributed to the enhanced rigidity of the polymer molecules that rely on the dispersion of the filler material in the polymer matrix. At higher percentage of filler loading, optimum dispersion is usually not attained, and particle agglomeration is due. In such case, the interaction between the polymer and the matrix is less which adversely affect the storage modulus.

Increases in the loss modulus can similarly be attributed to the polymer-particle interaction. As reported by

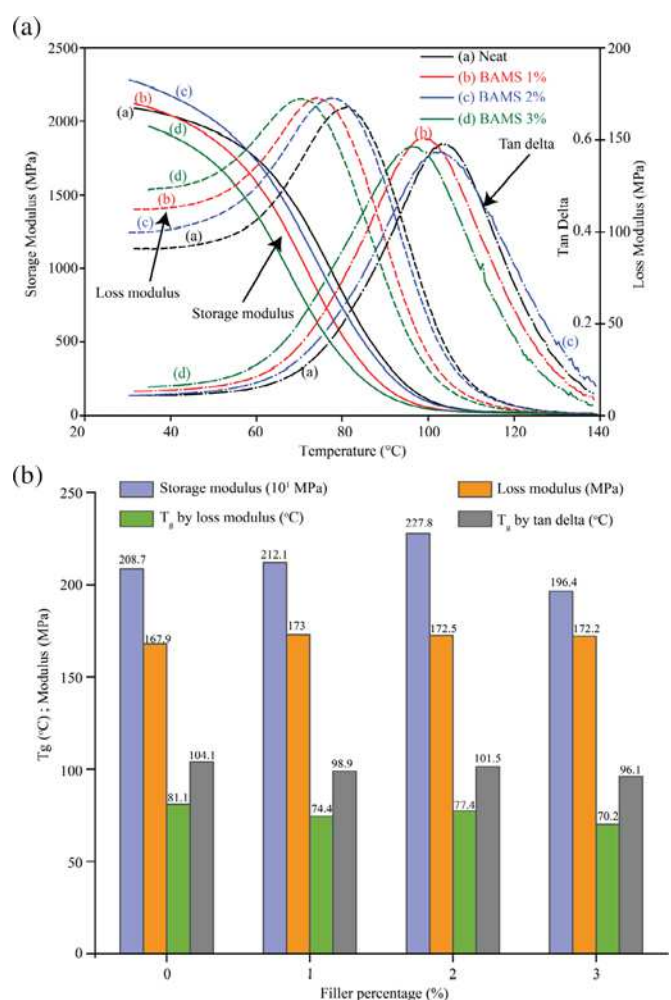


FIGURE 8 Summary of dynamic mechanical analysis (DMA) analysis: (a) DMA curves of the nanocomposites and (b) summary of the analysis of the DMA results for various filler percentages [Color figure can be viewed at wileyonlinelibrary.com]

others, ^{19,58,59} dispersion of the filler materials in the polymer matrix offers higher resistance against the movement of surrounding matrix, and thus results in high dissipation of energy.

Tan delta provides information about damping properties of the nanocomposites. It also gives a clear indication of T_g . The glass transition temperatures obtained from the tan delta follows similar qualitative trend as that of the glass transition temperatures obtained from DSC. As seen from the table, the T_g values are not much changed for all the nanocomposite systems. This is attributed to the presence of biobased content in Super Sap 100/1000 resin as discussed previously.

4 | CONCLUSION

In this work, we have successfully synthesized and characterized nanoparticles from the natural and renewable

source—bone ash. This was achieved by using simple techniques, such as mechanochemical attrition and ultrasound irradiation, in the synthesis process. The synthesized nanoparticles were characterized for their structure and particle size and found to be less than 50 nm retaining their crystal structure as revealed by XRD, SEM, and TEM. We were also successful in developing and characterizing the nanocomposites by incorporating our synthesized nanoparticles in a biobased epoxy, Super Sap 100/1000 system that contains up to 37% biomass. Flexural characterization reveals better flexural strength, flexural modulus, and toughness of the developed nanocomposites. This suggests that the incorporation of the nanoparticles into the epoxy system leads to good interaction between the particle and the polymer matrix. These results are complemented by the results from DMA which also showed improved storage modulus for all three nanoparticles, confirming better matrix-particle incorporation. In addition to that, TGA showed enhanced thermal stability, and TMA showed better dimensional stability in the developed nanocomposites. There are numerous scopes to work on in future. In order for finding the suitability in potential applications, barrier properties, flammability resistance, and other mechanical properties of the developed nanocomposites can be studied. In addition, environmental degradation and life cycle assessment of the nanocomposites should also be studied. Finally, fiber-reinforced nanocomposites with bone ash filler can be developed and studied for potential structural applications.

ACKNOWLEDGMENTS

The authors acknowledge the financial support of NSF-RISE #1459007, NSF-CREST#, 1735971 and NSF-MRI-1531934.

ORCID

Vijaya K. Rangari https://orcid.org/0000-0002-3962-1686

REFERENCES

- D. A. Hoornweg; L. Thomas; K. Varma What a Waste: Solid Waste Management in Asia; Urban and Local Government Working Paper, World Bank: Washington, DC, 1999.
- [2] D. Hoornweg; P. Bhada-Tata What a waste: a global review of solid waste management; Urban Development Series Knowledge Papers, World Bank: Washington, DC, **2012**.
- [3] M. Allsopp; A. Walters; D. Santillo; P. Johnston Plastic debris in the world's oceans; Greenpeace International: Amsterdam, Netherlands, 2006.
- [4] UN-HABITAT Solid Waste Management in the World's Cities: Water and Sanitation in the World's Cities 2010; Earthscan, **2010**.

- [5] H.-G. Ramke. Toolkit Landfill Technology; Landfill Technology: Höxter, Germany, **2009**.
- [6] Y. Macklin; A. Kibble; F. Pollitt Impact on Health of Emissions from Landfill Sites; Documents of the Health Protection Agency, 2011.
- [7] C. Bastioli, Handbook of Biodegradable Polymers, Rapra Technology, Shawbury, Shrewsbury, Shropshire, UK 2005.
- [8] L. Avérous, E. Pollet, Environmental silicate nano-biocomposites. in *Green Energy and Technology* (Eds: L. Avérous, E. Pollet), Springer London, London 2012.
- [9] B. Ghanbarzadeh, H. Almasi, in *Biodegradation-Life of Science* (Eds: R. Chamy, F. Rosenkranz), InTech, Rijeka, Croatia 2013, p. 141.
- [10] S. K. Kumar, R. Krishnamoorti, Annu. Rev. Chem. Biomol. Eng. 2010, 1, 37.
- [11] Y. Mai, Z. Yu, in *Polymer Nanocomposites* (Eds: Y. Mai, Z. Yu), Woodhead Publication, Boca Raton, FL 2006.
- [12] P. M. Ajayan, L. S. Schadler, P. V. Braun, Nanocomposite Science and Technology, Wiley, Verlag, Germany 2003.
- [13] B. Ellis, in *Chemistry and Technology of Epoxy Resins* (Ed: B. Ellis), Springer Netherlands, Dordrecht 1993.
- [14] N. Platzer, J. Polym. Sci. Part C Polym. Lett. 1987, 25, 268.
- [15] C. A. May, in *Epoxy Resins: Chemistry and Technology*, Second ed. (Ed: C. A. May), Marcel Dekker, New York, NY **1987**.
- [16] F. H. Chowdhury, M. V. Hosur, S. Jeelani, *Mater. Sci. Eng., A* 2006, 421, 298.
- [17] M. M. Rahman, M. Hosur, S. Zainuddin, K. C. Jajam, H. V. Tippur, S. Jeelani, *Polym. Test.* 2012, *31*, 1083.
- [18] N. Chisholm, H. Mahfuz, V. K. Rangari, A. Ashfaq, S. Jeelani, Compos. Struct. 2005, 67, 115.
- [19] M. M. Rahman, S. Zainuddin, M. V. Hosur, C. J. Robertson, A. Kumar, J. Trovillion, S. Jeelani, *Compos. Struct.* 2013, 95, 213.
- [20] H. Mahfuz, S. Zainuddin, M. R. Parker, T. Al-Saadi, V. K. Rangari, S. Jeelani, *Mater. Lett.* 2007, 61, 2535.
- [21] S. Zainuddin, M. V. Hosur, Y. Zhou, A. T. Narteh, A. Kumar, S. Jeelani, *Mater. Sci. Eng.*, A 2010, 527, 7920.
- [22] M. M. Rahman, S. Zainuddin, M. V. Hosur, J. E. Malone, M. B. A. Salam, A. Kumar, S. Jeelani, *Compos. Struct.* 2012, 94, 2397.
- [23] F. Pervin, Y. Zhou, V. K. Rangari, S. Jeelani, *Mater. Sci. Eng.*, *A* **2005**, 405, 246.
- [24] Y. Zhou, F. Pervin, M. A. Biswas, V. K. Rangari, S. Jeelani, Mater. Lett. 2006, 60, 869.
- [25] Y. Zhou, F. Pervin, L. Lewis, S. Jeelani, *Mater. Sci. Eng.*, A 2007, 452–453, 657.
- [26] Y. Zhou, F. Pervin, L. Lewis, S. Jeelani, Mater. Sci. Eng., A 2008, 475, 157.
- [27] Y. Zhou, F. Pervin, S. Jeelani, P. K. Mallick, J. Mater. Process. Technol. 2008, 198, 445.
- [28] Y. Zhou, F. Pervin, V. K. Rangari, S. Jeelani, *Mater. Sci. Eng.*, *A* **2006**, 426, 221.
- [29] R. Masoodi, R. F. El-Hajjar, K. M. Pillai, R. Sabo, *Mater. Des.* 2012, 36, 570.
- [30] R. Hoto, G. Furundarena, J. P. Torres, E. Muñoz, J. Andrés, J. A. García, *Mater. Lett.* **2014**, *127*, 48.
- [31] O. Faruk, A. K. Bledzki, H.-P. Fink, M. Sain, Prog. Polym. Sci. 2012, 37, 1552.
- [32] H. S. Jaggi, Y. Kumar, B. K. Satapathy, A. R. Ray, A. Patnaik, Mater. Des. 2012, 36, 757.

- [33] C. Albano, L. Cataño, R. Perera, A. Karam, G. González, Polym. Bull. 2010, 64, 67.
- [34] A. Pandey, E. Jan, P. Aswath, J. Mater. Sci. 2006, 41, 3369.
- [35] R. Roeder, J. Biomed. Mater. Res., Part A 2003, 67, 801.
- [36] Z. Hong, P. Zhang, A. Liu, J. Biomed. Mater. Res., Part A 2007, 81A, 515.
- [37] F. Asuke, V. S. Aigbodion, M. Abdulwahab, O. S. I. Fayomi, A. P. I. Popoola, C. I. Nwoyi, B. Garba, *Results Phys.* 2012, 2, 135.
- [38] I. A. Madugu, M. Abdulwahab, V. S. Aigbodion, J. Alloys Compd. 2009, 476, 807.
- [39] M. N. Cazaurang-Martinez, P. J. Herrera-Franco, P. I. Gonzalez-Chi, M. Aguilar-Vega, J. Appl. Polym. Sci. 1991, 43, 749.
- [40] B. C. Suddell, W. J. Evans, Natural Fibers, Biopolymers and Biocomposites, CRC Press, Boca Raton, FL 2005, p. 246.
- [41] K. G. Satyanarayana, K. Sukumaran, P. S. Mukherjee, C. Pavithran, S. G. K. Pillai, Cem. Concr. Compos. 1990, 12, 117.
- [42] S. He, K. Shi, J. Bai, Z. Zhang, L. Li, Z. Du, B. Zhang, *Polymer* 2001, 42, 9641.
- [43] L. A. Pothan, S. Thomas, N. R. Neelakantan, J. Reinf. Plast. Compos. 1997, 16, 744.
- [44] A. K. Mohanty, M. Misra, L. T. Drzal, J. Polym. Environ. 2002, 10, 19.
- [45] H. Gu, C. Ma, J. Gu, J. Guo, X. Yan, J. Huang, Q. Zhang, Z. Guo, J. Mater. Chem. C 2016, 4, 5890.
- [46] M. Tiwari, B. K. Billing, H. S. Bedi, P. K. Agnihotri, J. Appl. Polym. Sci. 2020, 137, 1.
- [47] I. O. Oladele, B. Makinde-Isola, J. Appl. Biotechnol. Bioeng. 2016, 1, 35.
- [48] D. S. Mahajan, T. D. Deshpande, M. L. Bari, U. D. Patil, J. S. Narkhede, J. Appl. Polym. Sci. 2020, 137, 1.

- [49] S. A. Nejad, G. H. Majzoobi, S. A. R. Sabet, Iran. Polym. J. 2019, 28, 895.
- [50] V. Agubra, P. Owuor, M. Hosur, Nanomaterials 2013, 3, 550.
- [51] ASTM Standard D790–10: Standard test methods for flexural properties of unreinforced and reinforced plastics and electrical insulating materials 2010.
- [52] ASTM Statndard D696 08e1: Standard test method for coefficient of linear thermal expansion of plastics between-30°C and 30°C with a vitreous silica dilatometer 2008, 08.
- [53] U. Gbureck, S. Dembski, R. Thull, J. E. Barralet, *Biomaterials* 2005, 26, 3691.
- [54] A. H. Roufosse, W. J. Landis, W. K. Sabine, M. J. Glimcher, J. Ultrastruct. Res. 1979, 68, 235.
- [55] J. Sim, Y. Kang, B. J. Kim, Y. H. Park, Y. C. Lee, *Polymers* 2020, 12, 1.
- [56] T. A. Nguyen, H. Nguyen, T. V. Nguyen, H. Thai, X. Shi, J. Nanosci. Nanotechnol. 2016, 16, 9874.
- [57] T. Hirata, P. Li, F. Lei, S. Hawkins, M. J. Mullins, H. J. Sue, J. Appl. Polym. Sci. 2019, 136, 1.
- [58] X. Liu, Q. Wu, L. A. Berglund, H. Lindberg, J. Fan, Z. Qi, J. Appl. Polym. Sci. 2003, 88, 953.
- [59] F. Lionetto, A. Maffezzoli, Appl. Rheol. 2009, 19, 23423.

How to cite this article: Uddin M-J, Kodali D, Rangari VK. Effect of bone ash fillers on mechanical and thermal properties of biobased epoxy nanocomposites. *J Appl Polym Sci.* 2021;138: e50046. https://doi.org/10.1002/app.50046